

High-Precision Magnetic Field Sensor Based on Fiber Bragg Grating and Dual-Loop Optoelectronic Oscillator

Wei SUN^{1,2}, Xiangyu LIU³, and Ming DENG^{3*}

¹State Key Laboratory of The Gas Disaster Detecting, Preventing and Emergency Controlling, Chongqing 400037, China

²China Coal Technology and Engineering Group Chongqing Research Institute, Chongqing 400039, China

³Key Laboratory of Optoelectronic Technology & Systems (Ministry of Education), Chongqing University, Chongqing 400044, China

*Corresponding author: Ming DENG E-mail: dengming@cqu.edu.cn

Abstract: A novel fiber-optic magnetic field sensor with high interrogation speed and resolution by using an etched fiber Bragg grating (FBG) in conjunction with a dual-loop optoelectronic oscillator (OEO) is proposed and experimentally demonstrated. A commercial FBG is firstly dipped into mixed hydrofluoric acid solution to remove the cladding layer and then is embedded with the magnetic fluid (MF) as a sensing element. The central wavelength reflected from the FBG is related to the overall time delay of the dual-loop OEO, which determines the oscillating frequency of the OEO. Therefore, the magnetic field can be estimated by measuring the oscillating frequency shift of OEO. The experimental results show that the oscillating frequency linearly increases with the increment of the magnetic field, achieving the sensitivity of 16.3 Hz/Oe with a *R*-square of 0.991 in the range of 5 mT–10 mT. In addition, the maximum error is within ± 0.05 mT in the range of 7 mT–8 mT, which offers potentials in many fields where the high-precision magnetic field measurement is required.

Keywords: Etched fiber Bragg grating; optoelectronic oscillator; magnetic fluid; magnetic field measurement

Citation: Wei SUN, Xiangyu LIU, and Ming DENG, "High-Precision Magnetic Field Sensor Based on Fiber Bragg Grating and Dual-Loop Optoelectronic Oscillator," *Photonic Sensors*, 2022, 12(4): 220419.

1. Introduction

Magnetic field sensors have been widely used in many scientific and industrial applications, including the biomedical detection, aviation industry, space and geophysical research, and controlled nuclear fusion [1–3]. Optical fiber magnetic field sensors have received special attention in the last years due to their outstanding advantages of immunity to electromagnetic interference, small size, remote sensing capabilities, and resistance in hazardous environments [4, 5]. In these sensors,

magneto-optical materials are crucial components which can interact directly or indirectly with the characteristic parameters of light. Especially, magnetic fluid (MF) is an exciting medium that possesses both magnetism like solid and fluidity like liquid material, as well as presents the magnetic field-dependent refractive index (RI) tunability [6]. As a result, various MF-based fiber structures have been developed for magnetic field measurement, mainly including the sensors based on the fiber Bragg grating (FBG) [7], fiber modal interferometer [8, 9], and fiber Fabry-Perot (FP) cavity [10].

Received: 25 February 2022 / Revised: 18 April 2022

© The Author(s) 2022. This article is published with open access at Springerlink.com

DOI: 10.1007/s13320-022-0662-9

Article type: Regular

Comparatively, the fiber magnetic field sensors based on MF and FBG are attractive in many applications due to excellent merits of intrinsic sensing elements, inherent self-reference, and unique multiplexing capability [11]. For example, Dai *et al.* [12] implemented a magnetic field sensor with the MF-coated etched FBG, obtaining the wavelength shift of 86pm in the range of 0–25 mT. Zheng *et al.* [13] reported a magnetic field sensor utilizing the MF-covered tilted FBG (TFBG), achieving magnetic field measurement within a range up to 19.6 mT by monitoring extinction ratio of the cladding mode. The most common approaches to interrogate the FBG-based magnetic field sensors are employing an optical spectrum analyzer (OSA) to monitor the change in the optical power or the resonance wavelength shift. Due to the poor resolution and slow scanning rate of OSA, the measurement precision and demodulation speed of the magnetic field sensors based FBG are accordingly low.

Optoelectronic oscillator (OEO) is a high- Q resonator whose operation involves both optical energy and microwave signals with pure spectra and low phase noise. The generated microwave signals shift in the OEO-based sensors can be monitored through a kind of digital signal processing (DSP) technique or an electric spectrum analyzer (ESA), which can effectively improve the interrogation speed and resolution. By applying the OEO technique to optical sensing fields, various OEO-based sensors have been demonstrated to achieve high-performance applications for different physical quantities, such as temperature [14], refractive index [15], strain [16], and trace copper [17]. For the magnetic field sensing, Wu *et al.* [18] proposed an OEO-based magnetic field sensor by using an FBG-FP filter. However, the structure of FBG-FP needs to be specially designed, and the sensing system requires two lasers, which increase the complexity and cost. Our group previously reported a temperature-compensated magnetic field sensor based on dual-loop OEOs incorporating the

cascaded magnetostrictive alloy-fiber Bragg grating (MA-FBG) and FBG filters [19]. In this case, the integration process of the magnetostrictive material with the optical fiber structure is not easy.

In this paper, a novel optical fiber magnetic field sensor based on a dual-loop OEO incorporating the MF-covered etched FBG is proposed. Since a dispersive element is included in the OEO loop, the oscillating frequency of the OEO is determined by the time delay of the optical and electrical links, which is as a function of the optical wavelength reflected from the FBG. So, the magnetic field can be measured by tracking the change in the oscillating frequency associated with the resonance wavelength variation of the MF-covered FBG induced by the external magnetic field. The experimental results show that the oscillating frequency linearly increases with the magnetic field enlarging from 5 mT to 10 mT, which presents the sensitivity of 16.3 Hz/Oe with the R -square of 0.991 and the maximum measurement error of within ± 0.05 mT in the range of 7 mT–8 mT. As a result, the proposed scheme has merits of simplicity and compact configuration, which can realize high-precision measurement with high interrogation speed.

2. Operation principles and sensor preparation

A dual-loop OEO can effectively suppress the side modes in each single loop, which can improve the system stability and sensing accuracy [20]. Hence, a dual-loop OEO scheme composed of a beam splitter and a beam combiner without adding any active electrical device in the sensing system is used as shown in Fig. 1. Firstly, the light from a broadband optical source (BOS) is fed into the sensing head consisting of an MF-coated etched FBG via an optical circulator (Cir). The optical source reflected by the above FBG is amplified by an erbium-doped fiber amplifier (EDFA), and then the amplified signal passes through a polarization

controller (PC) and is introduced into a Mach-Zehnder modulator (MZM). Next, the modulated signal is divided into two paths through an optical coupler (OC1), where one path passes through 1 km single mode fiber (SMF), and the other goes through a dispersion compensation fiber (DCF). The dispersion parameters of the SMF and DCF are 17 ps/nm and 83 ps/nm, respectively. Subsequently, the above two signals are combined after OC2 and sent to a photodetector (PD). In each loop, the signal process is equivalent to a single-loop OEO and a corresponding set of modes can be set up. Due to the gain competition between two sets of modes, only the modes that exist in each loop can oscillate. Therefore, the side modes are suppressed effectively. Finally, the output signal of the PD is amplified, filtered, and divided by an electrical amplifier (EA), an electrical bandpass filter (EBPF), and a power divider (DIV), respectively. One portion from DIV is detected by an electrical spectrum analyzer (ESA) to observe the oscillation frequency shift, and the other is sent back to the MZM to form the closed OEO loop.

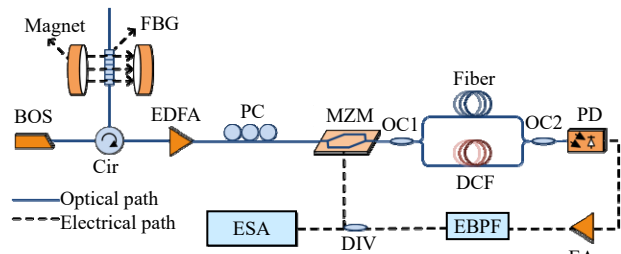


Fig. 1 Experimental system based on a dual-loop optoelectronic oscillator used for magnetic field sensing.

For the magnetic field sensor, the RI of the MF is dependent on the external magnetic field, thus, the effective RI of the FBG is significantly affected by the external RI change when the fiber cladding diameter is reduced to the grating region. As a result, the resonance wavelength of the MF clad etched FBG can shift with the change in the magnetic field, which can be expressed as

$$\Delta\lambda_B = 2\Delta n_{\text{eff}}A \quad (1)$$

where λ_B is the reflected wavelength of FBG. n_{eff} and

A are the effective RI and grating pitch, respectively.

Based on the principle of OEO system, the oscillating frequency is determined by the time delay of the whole optical and electrical links. Seen from Fig. 1, the time delay T consists of optical link and electrical link, which can be described as

$$T = T_e + T_o \quad (2)$$

where T_e denotes the delay time for the microwave signal to pass through the electrical link, and T_o is the delay time for the optical link, which includes DCF and SMF.

The free spectra range (FSR) of the generated electrical harmonic and the frequency of the N -th harmonic are described by (3) and (4) [21], respectively.

$$\text{FSR} = 1/T \quad (3)$$

$$f_N = N \cdot \text{FSR} = N/T. \quad (4)$$

When the resonance wavelength of the FBG shifts, the time delay in the optical link changes. Since the oscillation frequency is the mutual modes of two OEO loops, for simplicity, we only need to analyze the DCF loop. Provided that the additional time delay induced by the resonance wavelength shift $\Delta\lambda_B$ in the DCF is T_Δ , it can be written as

$$T_\Delta = D l_D \Delta\lambda_B \quad (5)$$

where D is the dispersion of the DCF. The oscillating frequency shift Δf can be depicted as (6). It can be found that the resonance wavelength change of the FBG induced by the external magnetic field can be converted to the drift of the OEO oscillating frequency. As a consequence, the magnetic field can be monitored by demodulating the microwave frequency variation.

$$\begin{aligned} \Delta f &= f_{N,\Delta\lambda} - f_N = \frac{N}{T + T_\Delta} - \frac{N}{T} = -\frac{NT_\Delta}{T(T + T_\Delta)} \\ &\approx -\frac{NT_\Delta}{T^2} = -\frac{NDl_D\Delta\lambda_B}{T^2}, \quad (T_\Delta \ll T). \end{aligned} \quad (6)$$

In order to enhance the interaction between the external magnetic field and the propagate core mode, a commercial FBG with the reflectivity of 95% and bandwidth of 0.2 nm is dipped into mixed hydrofluoric acid solution to remove the cladding

layer at room temperature. Here, the 40% hydrofluoric acid solution is diluted by ethanol and deionized water with 1:1:1 in volume. The diameter of the FBG is reduced by empirically controlling the etching time, and the etched FBG with the diameter of $\sim 15\ \mu\text{m}$ is prepared when taking robustness into account, as shown in Fig. 2(a). Then, the MF is slowly injected into a capillary containing the etched FBG to complete the magnetic sensing head preparation, as shown in Fig. 2(b). Figure 2(c) presents the reflectance spectra before etching (FBG), after etching (EFBG), and filling with the MF (EMFFBG), respectively. It can be noticed that the resonance wavelength shifts to the longer wavelength, which is mainly due to the change in the effective RI of the fiber core. In addition, the full width at a half maximum (FWHM) becomes narrower after being full of MF, which is easier to achieve highly precise magnetic field measurement.

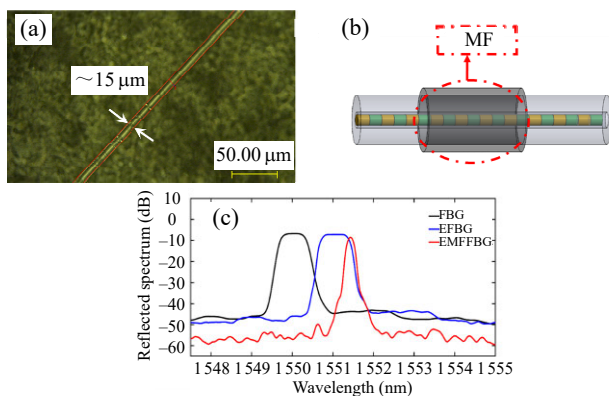


Fig. 2 Preparation and test of FBG-based magnetic field sensor: (a) micrograph of the etched FBG, (b) sensor encapsulation diagram, and (c) spectra before etching, after etching, and filling with MF.

3. Experimental results and discussion

An experiment is carried out to verify the concept and investigate the performance of the proposed scheme by using the setup as shown in Fig. 1. The MZM has a 10 GHz bandwidth and half-wave voltage of 6 V (TDKH1.5-10PD-ADC). The bandwidth of the PD is 15 GHz (CETC GD45220R). The central frequency and bandwidth of the EF are 942.5 MHz and 40 MHz (Spectrum

C942.5-40-6SS), respectively. A current source (CH-Hall, Model F2031) is used to drive a pair of Helmholtz coils to produce tunable magnetic field intensity, whose direction is perpendicular to the light wave vector and value is displayed on the magnetic field recorder by a Gauss meter (CH-Hall, Model 1500 Gauss/Tesla meter).

According to the sensing principle in Section 2, the MF clad etched FBG can be used to detect the magnetic field by measuring the resonance wavelength shift. When the magnetic field increases from 12 mT to 40 mT with a step of 4 mT, the spectral response is plotted in Fig. 3(a). It can be seen that the resonance wavelength generates blueshift with the increment of magnetic field because the RI of the MF decreases with the magnetic field expanding. The relationship of the measured wavelength shifts as a function of the magnetic field is depicted in Fig. 3(b). It can be found that 24 mT is a turning point of linear fitting sensitivity. The reason is that the RI of the MF has strong dependence on the magnetic particles, the base fluid, the concentration, the particles Brownian motion closely related to temperature, and the optical capture [22], and it can be described by the Langevin function [23], which shows the nonlinear function relationship between the RI of the MF and magnetic field intensity. The variation of RI of the MF can be roughly divided into hysteresis region, linear region with high sensitivity, and saturation region with low sensitivity. Given to the magnetic field value of 24 mT as the turning point of highly and lowly sensitive linear regions, the sensor sensitivities are characterized by the piecewise fitting method, which shows the measurement sensitivities of 2.6 pm/mT with the R -square of 0.992 in the range of 12 mT–24 mT, and 0.7 pm/mT with the R -square of 0.982 in the range of 24 mT – 40 mT, respectively.

Because the spectrometer used in our experiment (OSA, YOKOGAWA AQ6370D) has a minimum resolution of 20 pm, it is difficult to distinguish the

magnetic field variations when the change of the FBG wavelength caused by the external magnetic field is less than 20 pm. In order to achieve the magnetic field measurement with high resolution, the sensing parameter is interrogated by the OEO. Firstly, the OEO loop is closed, and then the OEO will begin to oscillate by adjusting the magnification factors of EDFA and EA to make the loop gain larger than 0 dB. Figure 4(a) shows the frequency spectrum of the generated 956.95 MHz signal with a side-mode suppression ration (SSR) of 29.6 dB, which is enough for accurate sensing application. In

addition, the stability of the oscillation frequency is a critical parameter for high precision measurement. Hence, we let the OEO system operating at the room temperature for a period of 30 minutes, whose oscillation frequency is recorded at the same time with a step of 2 mins, as shown in Fig. 4(b). The maximum frequency drift is 200 Hz, which may be attributed to the environmental perturbations (e.g., temperature and strain). The frequency shift measured above can present good robustness and meet experimental requirements.

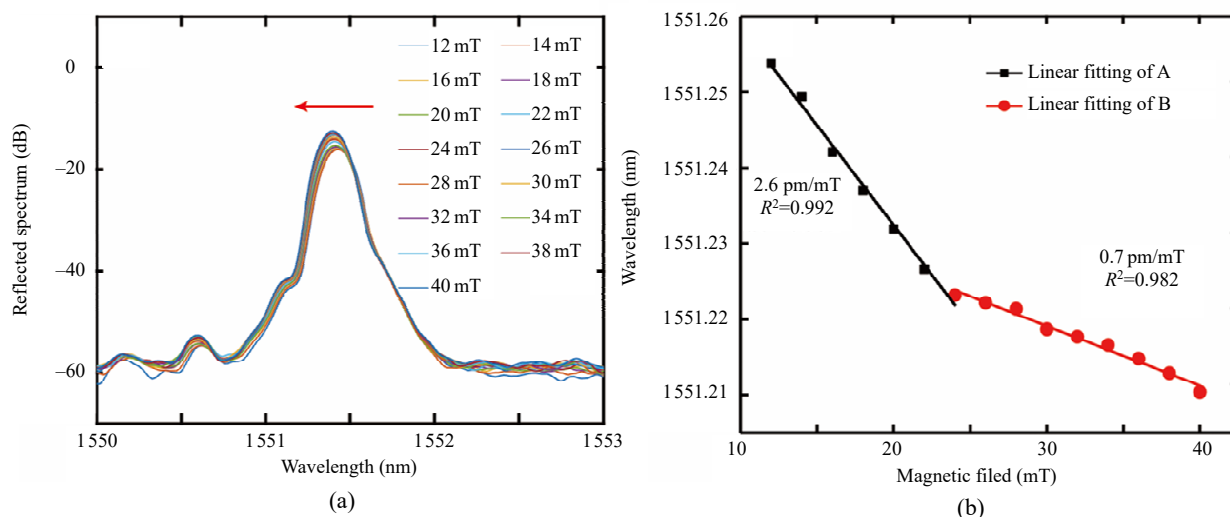


Fig. 3 Spectral response and sensitivity of the designed magnetic field sensor: (a) the measured spectra under different magnetic fields and (b) wavelength shift as a function of the magnetic field.

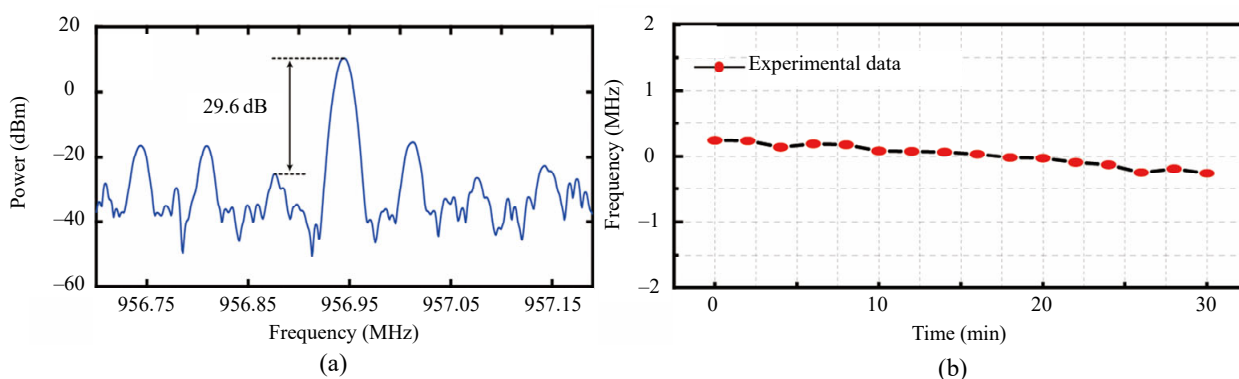


Fig. 4 Side-mode suppression ration and stability test of the designed dual-loop OEO: (a) electrical spectrum of the generated 956.95 MHz signal and (b) stability of the OEO at temporal duration of 30 mins.

The measured frequency responses of the OEO at different magnetic fields are drawn in Fig. 5(a). When the magnetic field increases from 0 to 10 mT

with a step of ~ 1 mT, the oscillation frequency shifts towards higher frequency, which is mainly because that the RI of the MF damps with the magnetic field

enlarging. Figure 5(b) describes the linear fitting relationship between the measured oscillation frequency and magnetic field, which reveals the sensitivity of 16.3 Hz/Oe with the *R*-square of 0.991 in the range of 5 mT–10 mT. It can be explained by the fact that the RI of the MF is not linearly changed under different magnetic fields. When the magnetic field intensity is less than 5 mT, the formation rate of

the magnetic chain is relatively small, resulting in the slight variation in the RI of the MF. Figure 5(c) represents the magnetic field measurement error of the designed sensing device, and a maximum measurement error of about ±0.05 mT is obtained, which indicates that the proposed sensing configuration has a huge prospect in the fields of precise magnetic field measurement.

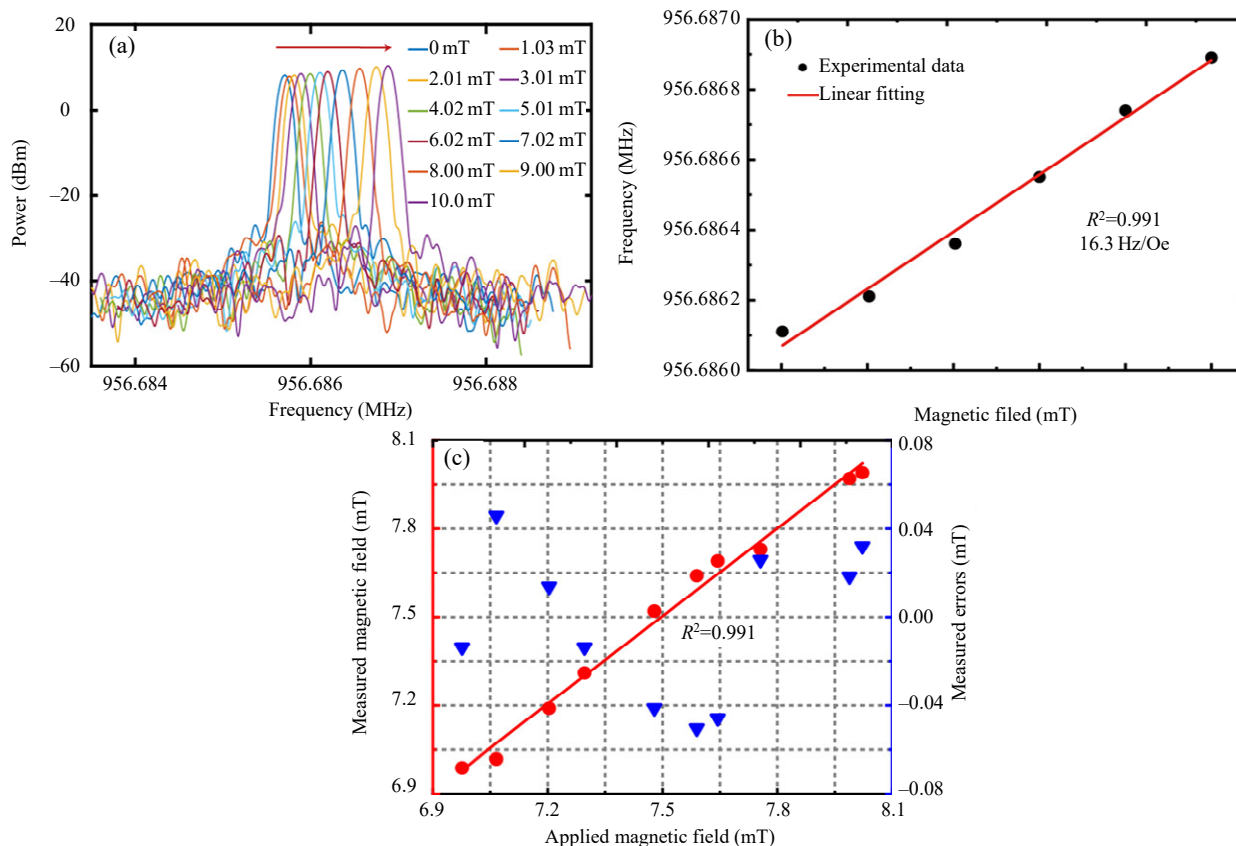


Fig. 5 Sensor performance characterization based on the etched FBG and the OEO: (a) the measured frequency responses under different magnetic fields, (b) relationship between the oscillating frequency shift and the magnetic field, and (c) the measured errors.

4. Conclusions

In this work, a highly sensitive fiber magnetic field sensor in combination with the etched FBG and the OEO is designed and demonstrated experimentally. Firstly, the magnetic field sensitivity of the designed sensor is characterized using the optical spectrum, and a maximum sensitivity of 2.6 pm/mT is achieved. In view of slow scanning speed and resolution of the spectrometer, the magnetic field sensitivity is estimated by measuring

the oscillating frequency shift of the OEO. The experimental results show that the oscillating frequency linearly increases with the increment of magnetic field, realizing the sensitivity of 16.3 Hz/Oe with a *R*-square of 0.991 in the range of 5 mT–10 mT. In addition, the maximum error is within ±0.05 mT in the range of 7 mT–8 mT, which offers potentials in many fields where the high-precision magnetic field measurement is required.

Acknowledgment

This work was supported by the National Natural Science Foundation of China (Grant No. 62075022), the Chongqing Technology Innovation and Development Project (Grant No. cstc2020jscxmsxmX0216), the Special Project of Science and Technology Innovation and Entrepreneurship Fund of Tiandi Technology Co., Ltd. (Grant No. 2020-TDZD007), and the Science and Technology Plan Project Support of Jiulongpo District (Grant No. 2020-02-004-Z).

Open Access This article is distributed under the terms of the Creative Commons Attribution 4.0 International License (<http://creativecommons.org/licenses/by/4.0/>), which permits unrestricted use, distribution, and reproduction in any medium, provided you give appropriate credit to the original author(s) and the source, provide a link to the Creative Commons license, and indicate if changes were made.

References

- [1] D. Shi, M. Sadat, A. Dunn, and D. Mast, "Photo-fluorescent and magnetic properties of iron oxide nanoparticles for biomedical applications," *Nanoscale*, 2015, 7(18): 8209–8232.
- [2] D. Toghraie, S. Alempour, and M. Afrand, "Experimental determination of viscosity of water-based magnetite nanofluid for application in heating and cooling systems," *Journal Magnetism and Magnetic Materials*, 2016, 417: 243–248.
- [3] Y. Zhao, X. Wang, R. Lv, G. Li, H. Zheng, and Y. Zhou, "Highly sensitive reflective Fabry-Perot magnetic field sensor using magnetic fluid based on Vernier effect," *IEEE Transactions on Instrumentation and Measurement*, 2021, 70: 1–8.
- [4] Z. Li, C. Liao, J. Song, Y. Wang, F. Zhu, Y. Wang, *et al.*, "Ultrasensitive magnetic field sensor based on an in-fiber Mach-Zehnder interferometer with a magnetic fluid component," *Photonics Research*, 2016, 4(5): 197–201.
- [5] N. Alberto, M. Domingues, C. Marques, P. Andre, and P. Antunes, "Optical fiber magnetic field sensors based on magnetic fluid: a review," *Sensors*, 2018, 18(12): 4325.
- [6] P. Li, H. Yan, Z. Xie, Y. Li, and X. Zhao, "An intensity-modulated and large bandwidth magnetic field sensor based on a tapered fiber Bragg grating," *Optics and Laser Technology*, 2020, 125: 105996.
- [7] J. Zheng, X. Dong, P. Zu, L. Shao, C. Chan, Y. Cui, *et al.*, "Magnetic field sensor using tilted fiber grating interacting with magnetic fluid," *Optics Express*, 2013, 21(15), 17863–17868.
- [8] Y. Luo, X. Lei, F. Shi, and B. Peng, "A novel optical fiber magnetic field sensor based on Mach-Zehnder interferometer integrated with magnetic fluid," *Optik*, 2018, 174: 252–258.
- [9] H. Zhang, Y. Li, B. Yuan, L. Meng, F. Cheng, Z. Yuan, *et al.*, "Magnetic field sensor based on S-shaped and core-offset fusion splicing structure of single-mode fiber coated with magnetic fluid," *Optik*, 2021, 245: 167630.
- [10] Z. Ruan, L. Pei, T. Ning, J. Wang, J. Wang, J. Li, *et al.*, "Simple structure of tapered FBG filled with magnetic fluid to realize magnetic field sensor," *Optical Fiber Technology*, 2021, 67: 102698.
- [11] P. Zu, C. Chan, W. Lew, L. Hu, Y. Jin, H. Liew, *et al.*, "Temperature-insensitive magnetic field sensor based on nanoparticle magnetic fluid and photonic crystal fiber," *IEEE Photonics Journal*, 2012, 4(2): 491–498.
- [12] J. Dai, M. Yang, X. Li, H. Liu, and X. Tong, "Magnetic field sensor based on magnetic fluid clad etched fiber Bragg grating," *Optical Fiber Technology*, 2011, 17(3): 210–213.
- [13] J. Zheng, X. Dong, P. Zu, L. Shao, C. Chan, Y. Cui, *et al.*, "Magnetic field sensor using tilted fiber grating interacting with magnetic fluid," *Optics Express*, 2013, 21(15): 17863–17868.
- [14] Y. Zhu, X. Jin, H. Chi, S. Zheng, and X. Zhang, "High-sensitivity temperature sensor based on an optoelectronic oscillator," *Applied Optics*, 2014, 53(22): 5084–5087.
- [15] Q. Shi, Y. Wang, Y. Cui, W. Xia, D. Guo, and M. Wang, "Resolution-enhanced fiber grating refractive index sensor based on an optoelectronic oscillator," *IEEE Sensors Journal*, 2018, 18(23): 9562–9567.
- [16] Z. Fan, J. Su, T. Zhang, N. Yang, and Q. Qiu, "High-precision thermal-insensitive strain sensor based on optoelectronic oscillator," *Optics Express*, 2017, 25(22): 27037.
- [17] M. Deng, X. Liu, D. Feng, Y. Tang, and T. Zhu, "Trace copper detection using in-line optical fiber Mach-Zehnder interferometer combined with an optoelectronic oscillator," *Optics Express*, 2021, 29(15): 23430.
- [18] B. Wu, M. Wang, Y. Dong, Y. Tang, H. Mu, H. Li, *et al.*, "Magnetic field sensor based on a dual-frequency optoelectronic oscillator using cascaded magnetostrictive alloy-fiber Bragg grating-Fabry Perot and fiber Bragg grating-Fabry Perot filters," *Optics Express*, 2018, 26(21): 27628.
- [19] D. Feng, Y. Gao, T. Zhu, M. Deng, X. Zhang, and L. Kai, "High-precision temperature compensated magnetic field sensor based on optoelectronic oscillator," *Journal of Lightwave Technology*, 2021,

- 39(8): 2559–2564.
- [20] X. Zou, X. Liu, W. Li, P. Li, W. Pan, L. Yan, *et al.*, “Optoelectronic oscillators (OEOs) to sensing, measurement, and detection,” *IEEE Journal of Quantum Electronics*, 2016, 52(1): 0601116.
- [21] J. Yang, J. Yu, Y. Wang, L. Zhang, and E. Yang, “An optical domain combined dual-loop optoelectronic oscillator,” *IEEE Photonics Technology Letters*, 2007, 19(11): 807–809.
- [22] M. Osaci and M. Cacciola, “Study about the nanoparticle agglomeration in a magnetic nanofluid by the Langevin dynamics simulation model using an effective Verlet-type algorithm,” *Microfluidics and Nanofluidics*, 2019, 21(2): 19.
- [23] Y. Chen, S. Yang, W. Tse, H. Horng, C. Hong, and H. Yang, “Thermal effect on the field-dependent refractive index of the magnetic fluid film,” *Applied Physics Letters*, 2003, 82(20): 3481–3483.